JOURNAL OF THERMOPHYSICS AND HEAT TRANSFER
Vol. 24, No. 1, January–March 2010

Analytical Method for Determining Heat Flux from Temperature-Sensitive-Paint Measurements in Hypersonic Tunnels

Tianshu Liu*
Western Michigan University, Kalamazoo, Michigan 49008
Zemin Cai†
Shantou University, 515063 Shantou, People's Republic of China
Jianhuang Lai‡
Sun Yat-sen University, 510275 Guangzhou, People's Republic of China
and
Justin Rubal§ and John P. Sullivan¶
Purdue University, West Lafayette, Indiana 47907

DOI: 10.2514/1.43372

This paper describes the analytical method used for temperature-sensitive-paint measurements to obtain quantitative global heat flux diagnostics in hypersonic tunnels. An exact inverse solution of the one-dimensional unsteady heat conduction equation for a polymer layer (temperature-sensitive paint or temperature-sensitive paint and an insulator layer) on a base of any material is obtained to calculate heat flux into the polymer surface as an explicit function of a time-dependent surface temperature change measured by temperature-sensitive paint. In addition, an analytical solution of the three-dimensional unsteady heat conduction equation is given to consider the effect of the lateral heat conduction. Simulations and experiments are conducted to examine the analytical method and assess the relevant factors regarding the measurement uncertainty.

I. Introduction

HEAT transfer to a hypersonic vehicle surface is one of the most important aerothermodynamic quantities and one that often remains difficult to predict using modern computational fluid dynamics. Global heat transfer measurement is particularly critical to a deep understanding of relevant phenomena such as transition, near-surface stationary vortices, and separation. Arrays of thermocouples have been used to measure heat transfer on a model. However, due to the limited spatial resolution of the array, critical effects are often difficult or impossible to capture. Temperature-sensitive paint (TSP) provides a useful tool for quantitative global heat transfer diagnostics in hypersonic tunnels [1–7]. TSP is a thin polymer layer doped with certain luminescent molecules for which the emission is sensitive to temperature. Therefore, once TSP coated on a surface is calibrated, surface temperature fields can be measured by detecting the luminescent emission from TSP [8]. TSP is usually airbrushed directly on a model surface or a surface of an insulating layer used to coat a metal model. Illumination lights with a suitable wavelength are used to excite TSP. Digital cameras with optical filters are used to image TSP. After a time sequence of the surface temperature fields is obtained from TSP in a hypersonic tunnel, the main problem is how to accurately extract a heat flux field on a model surface. Heat transfer measurements using conventional local gauges such as thin-film thermocouples in hypersonic tunnels have been comprehensively described by Schultz and Jones [9]. In contrast, methods for calculation of heat flux from TSP measurements are not given in a systematical and general fashion. In particular, TSP as a polymer layer alters a history of the surface temperature, and therefore the effect of TSP itself on heat flux calculation should be addressed.

A simple method for calculating heat flux is the use of the discrete Fourier law, which has been used for heat transfer data reduction in TSP measurements in hypersonic tunnels because it is simple and reasonably accurate for high-conductive bases [1,2,5]. Another method is based on the transient solution of the one-dimensional (1-D) time-dependent heat conduction equation. To process thermographic phosphor data, Merski [10,11] has used an analytical solution of the 1-D time-dependent heat conduction equation to a step change of heat transfer on a semi-infinite body assuming that heat flux is proportional to the enthalpy difference between the adiabatic wall and real model wall. Because a model is injected to the tunnel, the model does not experience an ideal step function of time in heat transfer. Thus, an effective time is introduced. In addition, the thermal diffusivity depending on temperature and adiabatic wall enthalpy are estimated. The heat conduction equation can be directly solved using a finite difference or finite element method when the measured temperature fields are given as a boundary condition. Thus, heat flux on the surface can be calculated. However, this forward numerical calculation of the temperature gradient is sensitive to the uncertainty of surface temperature measurement. In fact, the determination of heat flux from measured temperature fields is generally considered as an inverse heat transfer problem [12,13]. The inverse method has been compared with other methods by Walker and Scott [14] for thermocouples. The inverse method has been used for IR cameras [15], TSP [16], and general thermographic data [17].

This paper gives a simple and robust analytical method for calculating heat flux from TSP measurements. Because a TSP layer is a polymer layer, a combination of a TSP layer and a thermal resistance layer is treated as a single polymer layer. The fundamental heat transfer problem for TSP measurements in hypersonic flow is to extract heat flux into a thin polymer layer on a large base from a time

Presented as Paper 0736 at the 47th AIAA Aerospace Sciences Meeting, Orlando, FL, 5–8 January 2009; received 21 January 2009; revision received 30 June 2009; accepted for publication 9 July 2009.

*Professor, Department of Mechanical and Aeronautical Engineering, Room G-220, Parkview Campus; tianshu.liu@wmich.edu. Senior Member AIAA (Corresponding Author).
†Associate Professor, Department of Electrical and Electronic Engineering.
‡Professor, School of Information Science and Technology.
§Graduate Research Assistant, School of Aeronautics and Astronautics.
¶Professor, School of Aeronautics and Astronautics.

history of the surface temperature measured by TSP. The thin polymer could be TSP itself or TSP plus an insulator layer (for example, Mylar sheet) with a suitable thickness. Compared with the polymer layer, the thickness of a base is much larger, such that a semi-infinite base can be used as a good approximation. Figure 1 shows a thin polymer layer with a thickness covered on a semi-infinite base. A model in hypersonic testing is typically made of metals such as stainless steel and aluminum that have much larger thermal conductivity than a polymer. Low-thermal-conductive ceramic and nylon models are also used. First, an exact solution for the constant thermal properties is given by applying the inverse Laplace transform to the problem. The discrete form of the solution, which is a generalization of the Cook–Felderman method, can be used to calculate heat flux from a time history of the surface temperature. An analytical solution of the 3-D heat conduction equation is also sought by using the Fourier transform and Laplace transform to consider the effect of the lateral heat conduction. The developed method is examined in simulations and experiments.

II. Analytical Method for Determination of Heat Flux from TSP Data

The transient solution of the 1-D time-dependent heat conduction equation is sought for a thin polymer (TSP or TSP/insulator) on a semi-infinite base. An exact solution for a polymer on a base of an arbitrary material is derived by inverting the Laplace transform in Appendix A, and it is used as a general method for calculation of heat flux from TSP data. The heat flux at the polymer surface is given by

$$q_s(t) = \frac{k_p(1-\bar{\varepsilon}^2)}{\sqrt{\pi a_p}} \int_0^t \frac{\bar{W}(t-\tau,\bar{\varepsilon})}{\sqrt{t-\tau}} \frac{\mathrm{d}\theta_{ps}(\tau)}{\mathrm{d}\tau}\,\mathrm{d}\tau \tag{1}$$

where $\theta_{ps}(t) = T(t,L) - T_{\text{in}}$ is the temperature change at the polymer surface from the initial temperature T_{in}, L is the polymer-layer thickness, and

$$\bar{W}(t,\bar{\varepsilon}) = \frac{2}{\sqrt{\pi}} \int_0^\infty \frac{\exp(-\xi^2)\mathrm{d}\xi}{1+\bar{\varepsilon}^2 - 2\bar{\varepsilon}\cos(2L\xi/\sqrt{a_p t})} \tag{2}$$

The parameter $\bar{\varepsilon}$ is defined as $\bar{\varepsilon} = (1-\varepsilon)/(1+\varepsilon)$, where $\varepsilon = \sqrt{k_p\rho_p c_p / k_b\rho_b c_b}$ (k_p, c_p, and ρ_p are the thermal conductivity, specific heat and density of the polymer, respectively, k_b, c_b and ρ_b are the thermal conductivity, specific heat, and density of the base material, respectively), and $a_p = k_p/c_p\rho_p$ is the thermal diffusivity of the polymer. For $\bar{\varepsilon} = 0$, Eq. (1) recovers the classical solution for a semi-infinite base since $\bar{W}(t,0) = 1$. This means that the function $\bar{W}(t,\bar{\varepsilon})$ represents the effect of the polymer layer (or TSP itself) on the determination of heat flux, which depends on $\bar{\varepsilon}$, a_p, and L.

The discrete form of Eq. (1) for actual calculation of heat flux is

$$q_s(t_n) \cong \frac{k_p(1-\bar{\varepsilon}^2)}{\sqrt{\pi a_p}} \sum_{i=1}^{n} \frac{\theta_{ps}(t_i) - \theta_{ps}(t_{i-1})}{\sqrt{t_n - t_i} + \sqrt{t_n - t_{i-1}}} [\bar{W}(t_n - t_i) + \bar{W}(t_n - t_{i-1})] \tag{3}$$

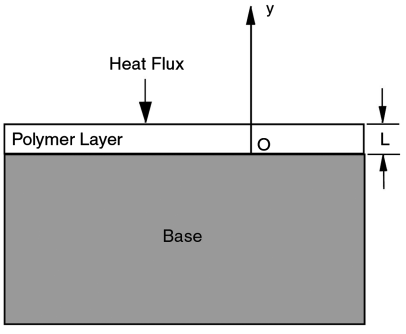

Fig. 1 Thin polymer layer on a semi-infinite base and a coordinate system.

Equation (3) can be considered as a generalization of the Cook–Felderman method for a combination of a polymer layer and a semi-infinite base of any material. Like the Cook–Felderman method [18], the numerical scheme, Eq. (3), is easy to implement in applications.

III. Effect of Lateral Heat Conduction

The analysis based on the 1-D heat conduction equation assumes that the lateral heat conduction can be neglected. To evaluate the effect of the lateral heat conduction, the 3-D heat conduction equations for a polymer layer and a semi-infinite base are solved by using a combination of the Fourier transform and the Laplace transform (see Appendix A). A similar treatment of the lateral heat conduction is given by Estorf [17]. In this case, we obtain the heat flux into the surface of the polymer layer:

$$q_s(t) = \frac{k_p(1-\bar{\varepsilon}^2)}{\sqrt{\pi a_p}} \left[\int_0^t \frac{\bar{W}(t-\tau,\bar{\varepsilon})}{\sqrt{t-\tau}} \frac{\mathrm{d}\langle\theta_{ps}\rangle_{g_1}(\tau)}{\mathrm{d}\tau}\,\mathrm{d}\tau + \int_0^t \frac{\bar{W}(t-\tau,\bar{\varepsilon})}{\sqrt{t-\tau}} \langle\theta_{ps}\rangle_{g_2}(\tau)\,\mathrm{d}\tau \right] \tag{4}$$

where the spatially filtered (averaged) temperature changes are

$$\langle\theta_{ps}\rangle_{g_1} = \int_{-\infty}^{\infty}\int_{-\infty}^{\infty} g_1(x-x', z-z', t-\tau)\theta_{ps}(\tau,x',z')\,\mathrm{d}x'\,\mathrm{d}z' \tag{5}$$

$$\langle\theta_{ps}\rangle_{g_2} = \int_{-\infty}^{\infty}\int_{-\infty}^{\infty} g_2(x-x', z-z', t-\tau)\theta_{ps}(\tau,x',z')\,\mathrm{d}x'\,\mathrm{d}z' \tag{6}$$

The filter functions g_1 and g_2 are defined as

$$g_1(x,z,t) = \frac{1}{4\pi a_p t} \exp\left(-\frac{x^2+z^2}{4a_p t}\right) \tag{7}$$

$$g_2(x,z,t) = \frac{1}{4\pi a_p t^2} \left(1 + \frac{x^2+z^2}{4a_p t}\right) \exp\left(-\frac{x^2+z^2}{4a_p t}\right) \tag{8}$$

The functions g_1 and g_2 are the Gaussian filter and modified Gaussian filter, respectively. Equation (4) has a similar form to Eq. (1) for the 1-D case, except for an additional integral term related to the filtered temperature change based on g_2. The lateral heat conduction is characterized by the size of the filter functions for the averaged temperature change, and the standard deviation $\sqrt{2a_p t}$ defines the affected region. For Mylar, $\sqrt{2a_p t} \approx 4.4 \times 10^{-4}\sqrt{t}$, and therefore $\sqrt{2a_p t} \approx 0.62$ mm at $t = 2$ s. When heat flux does not drastically change in a small circular region of 0.62 mm, the 1-D solution equation (1) is sufficiently accurate. In the limit case, when $\sqrt{2a_p t} \to 0$, then g_1 approaches the Dirac delta function $\delta(x,z)$, and Eq. (4) is reduced to Eq. (1).

IV. TSP Surface Temperature and TSP-Measured Temperature

In the preceding analysis, the temperature $T_{ps}(t)$ at a TSP surface is presumably known as a boundary condition. However, $T_{ps}(t)$ does not equal the TSP-measured temperature, and this difference has not been considered in previous measurements. Because a camera detects the integrated luminescent intensity across a thin TSP layer, the surface temperature measured by using TSP is an averaged temperature across the TSP layer; that is,

$$T_{\text{TSP}}(t) = L_{\text{TSP}}^{-1} \int_0^{L_{\text{TSP}}} T(t,y)\,\mathrm{d}y \tag{9}$$

where L_{TSP} is the thickness of the TSP layer. Using a Taylor expansion

$$T(t, y) \approx T_{ps} + (y - L_{\text{TSP}})\partial T/\partial y|_{y=L_{\text{TSP}}}$$

at the TSP surface and $q_s = k_p \partial T/\partial y$ into the TSP layer, we have an iterative relation:

$$T_{ps}^{(n+1)}(t) = T_{\text{TSP}}(t) + 0.5 q_s^{(n)}(t) L_{\text{TSP}}/k_p \tag{10}$$

Because the heat flux into the surface is considered to be positive here, $T_{ps}(t)$ is always larger than $T_{\text{TSP}}(t)$, depending on the heat flux and the thickness of the TSP layer. Equation (10) is used as an iterative correction scheme. For an initial guess $T_{ps}^{(0)}(t) = T_{\text{TSP}}(t)$, an estimate of $q_s(t)$ can be obtained from the preceding analytical method. Then a corrected $T_{ps}(t)$ is given by using Eq. (10) and an improved $q_s(t)$ is obtained. Usually, the temperature correction is required for high heat flux, and three iterations lead to a convergent result.

V. Simulations

A. Recovered Results for Modeled Starting Processes

To examine the general analytical solution, we consider a polyvinyl chloride (PVC) layer on semi-infinite bases made of aluminum and nylon 6. A step change followed by a sinusoidal variation in heat flux are used as a preliminary model of the transient starting process in The Boeing Company and U.S. Air Force Office of Scientific Research (AFOSR) Mach-6 Quiet Tunnel at Purdue University, as shown in Fig. 2. Table 1 lists the thermal properties of these materials commonly used for models and polymer layers in hypersonic testing. In simulations, aluminum and nylon 6 are used as typical high- and low-conductive materials for models, respectively. Usually, TSP has similar thermal properties to those of PVC. The time history of temperature on a 0.01-mm-thick PVC surface on a semi-infinite aluminum base is generated by solving the unsteady 1-D heat conduction equation using a forward-time, centered-space, finite difference scheme. Typically, the numbers of points selected in the polymer layer and base are 20 and 500, respectively. The number of points selected in the time domain varies from 501 to 4001, depending on the time interval and the properties of materials.

Figure 3 shows the resulting temperature histories responding to the simulated heat flux. Then the heat flux history is recovered by using the general method Eq. (3), and excellent agreement with the simulated one is achieved, as shown in Fig. 4. The parallel simulations are conducted for a 0.01-mm-thick PVC layer on a nylon 6 base. Figures 5 and 6 show the corresponding results. The system of the PVC layer on the nylon 6 base has a larger characteristic timescale than that of the PVC with the aluminum base. In calculations, the numbers of points in the time domain for the PVC layer on the Al and nylon 6 bases are 501 and 4001, respectively. A question is whether a different starting process alters the recovered heat flux using the general method because hypersonic facilities have different starting behaviors. The linear and the random starting processes have been also examined [19]. It is found that they do not affect the recovered heat flux almost immediately after the transient process.

Table 1 Thermal properties of polymer and base materials

	Mylar	PVC	Al	Stainless steel	Nylon 6	Macor
k, W/m · K	0.15	0.16	204	16	0.25	1.5
ρ, kg/m^3	1420	1300	2700	7900	1140	2520
c_p, J/kg · K	1090	900	904	500	1670	790

B. Error Analysis

The sensitivity analysis is given to assess the uncertainty of heat flux recovered by the general method, which depends on the elemental error sources in the parameters L, k_p, $\bar{\varepsilon}$, and a_p. For a simulated step heat flux ($q_s = 3000$ W/m^2 for $t > 0$), the uncertainty $\Delta q_s/q_s$ is estimated as a function of the elemental errors $\Delta L/L$, $\Delta k_p/k_p$, $\Delta\bar{\varepsilon}/\bar{\varepsilon}$, and $\Delta a_p/a_p$ for a 0.05-mm-thick PVC layer on a semi-infinite aluminum and nylon 6 bases, as shown in Fig. 7.

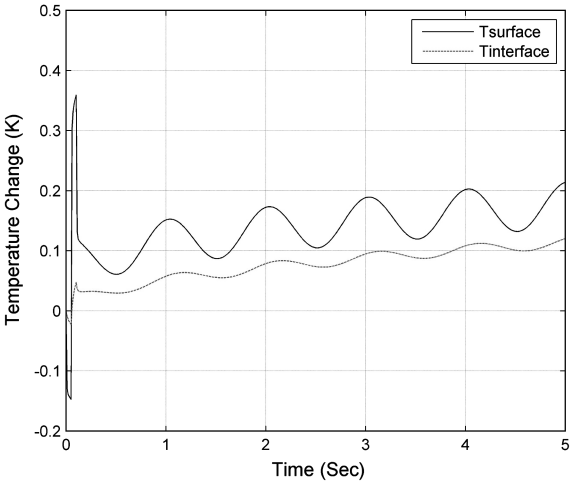

Fig. 3 Temperature histories at the PVC surface and interface between the 0.01-mm-thick PVC sheet and a semi-infinite aluminum base, responding to the simulated heat flux.

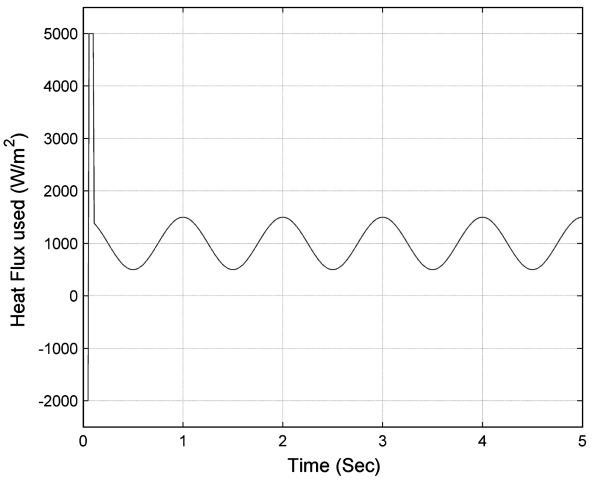

Fig. 2 Simulated heat flux with starting step changes followed by a sinusoidal change.

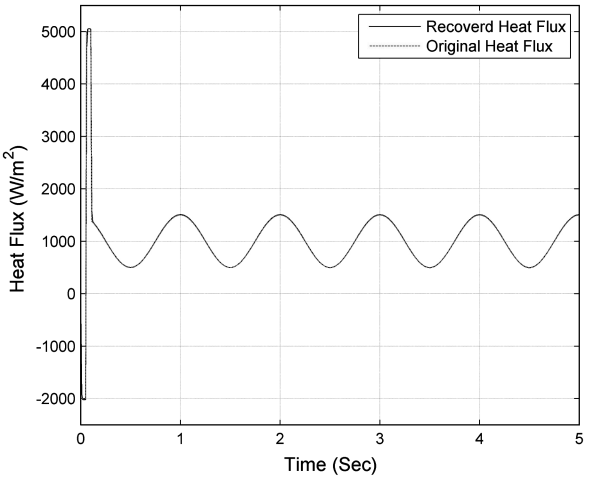

Fig. 4 Comparison of the recovered heat flux using the general method with the given one for a 0.01 mm PVC layer on a semi-infinite aluminum base.

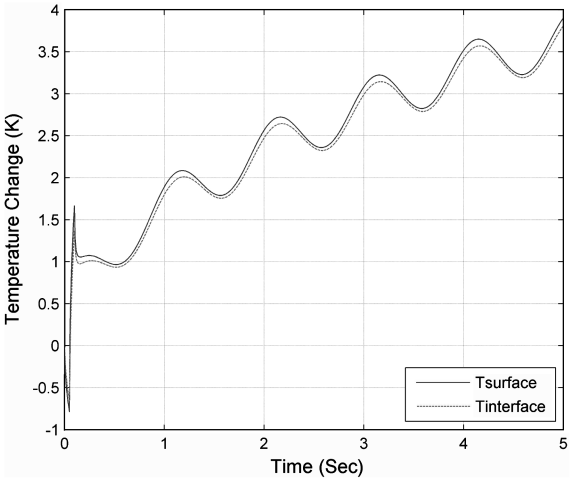

Fig. 5 Temperature histories at the Mylar surface and interface between the 0.01-mm-thick PVC sheet and a semi-infinite nylon 6 base, responding to the simulated heat flux.

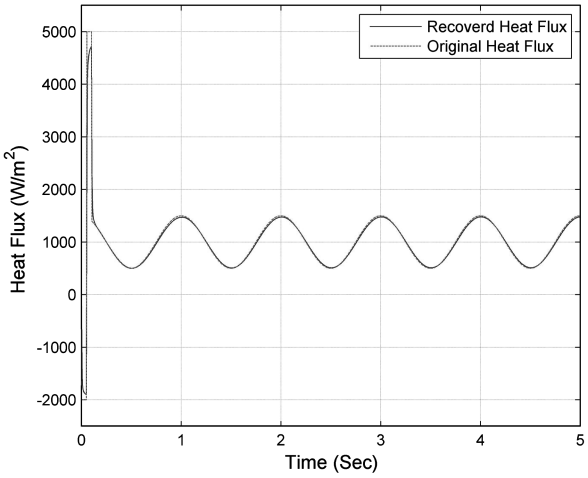

Fig. 6 Comparison of the recovered heat flux using the general method with the given one for a 0.01 mm PVC layer on a semi-infinite nylon 6 base.

The sensitivity of $\Delta q_s/q_s$ to the elemental error $\Delta L/L$ in the polymer thickness is weak for the PVC layer on the nylon 6 base. This consequence can be directly drawn from Eq. (2), in which the effect of L is limited in the term $\bar{\varepsilon}\cos(2L\xi/\sqrt{a_p t})$. Clearly, for a low-conductive base such as nylon 6 in which $\bar{\varepsilon}$ is small, a change of L will cause a relatively small effect on the calculated heat flux q_s. In contrast, for the PVC layer on the aluminum base, $\Delta q_s/q_s$ is sensitively dependent on $\Delta L/L$. In addition, $\Delta q_s/q_s$ is weakly dependent on $\Delta k_p/k_p$ and $\Delta\bar{\varepsilon}/\bar{\varepsilon}$ for the nylon 6. The dependency of $\Delta q_s/q_s$ on $\Delta a_p/a_p$ is very weak for both aluminum and nylon 6. According to the preceding sensitivity analysis, when the thermal properties of the materials and the polymer-layer thickness cannot be measured accurately, a low-conductive base is the preferred choice. For the aluminum base, however, accurate measurements of the polymer-layer thickness and the thermal properties are more critical to calculation of q_s.

The uncertainty in surface temperature measurements will lead to the uncertainty in calculation of heat transfer, which consists of a random error and a bias error of temperature. Although a random error in temperature propagates to the heat flux through the calculation, it is indicated that the random error in temperature does not produce a significant bias error in the time-averaged heat flux [19]. In other words, time averaging or ensemble averaging will remove the effect of a random error. Further, the effect of a bias error of temperature on the determination of heat flux is examined. The linear dependence of the relative error in heat flux on the relative error in temperature is found in simulations.

In measurements in short-duration hypersonic tunnels, a small group of sample points in a temperature history is often obtained, due to a limited rate of frames of a camera. In this case, heat flux calculation by using Eq. (3) has a greater numerical error because the time interval in the numerical integration is larger. For a simulated step heat flux ($q_s = 3000$ W/m^2 for $t > 0$), 501 points in temperature in a time period of 5 s for a 0.1-mm-thick PVC layer on a semi-infinite nylon 6 are generated numerically. As shown in Fig. 8, a significant bias error in heat flux calculation is found for 21 sample points. To solve this problem, a third-order polynomial fit to 21 sample points is applied, and 501 interpolated points are used to calculate heat flux by using Eq. (3). As also shown in Fig. 8, the significantly improved result is obtained simply based on the suitable interpolation to the temperature data. A larger error in the transient process is due to the fitting error. Furthermore, the recovered heat flux in the transient process is not accurate because the step change in heat flux cannot be truly recovered, due to the intrinsic thermal inertia of a polymer layer and a base. For a 0.1-mm-thick PVC layer on a semi-infinite aluminum, the recovered heat flux is very close to the true value even for 11 sample points after the transient starting process. In this case, the time evolution of the surface temperature is so gradual that a reasonable result can be obtained even though sample points are small.

VI. Experiments

A. 48-Inch Shock Tunnel

To examine the proposed analytical method, we reprocess raw TSP images on the sharp 25 deg /45 deg indented cone model obtained by Hubner et al. [2] in run 46 at Mach 11 in the 48 in. shock tunnel at Calspan–University of Buffalo Research Center. The detailed description of the experiments is given by Hubner et al. [2], and only data relevant to heat flux calculation using the analytical method are given here. Over 60 platinum thin-film heat transfer gauges were installed along a ray of the model, providing heat flux data for comparison with TSP. The reported measurement accuracy of the gauges is $\pm 5\%$, and the measurement resolution is 5 kW/m^2. TSP was Ru(phen) in a non-oxygen-permeable polyurethane binder. The TSP calibration data are fit by a polynomial:

$$\frac{T}{T_{\text{ref}}} = \sum_{n=0}^{8} a_n \left[\ell_n \frac{I_{\text{ref}}}{I}\right]^n$$

where $a_0 = 1.0$, $a_1 = 0.1167$, $a_2 = 0.0853$, $a_3 = -0.1404$, $a_4 = -0.2186$, $a_5 = 0.498$, $a_6 = -0.3386$, $a_7 = 0.0996$, and $a_8 = -0.0109$. The reference temperature T_{ref} was 295 K. The thickness of TSP was 10 μm, and the white polyurethane basecoat was 40 μm. Thus, the total thickness of the polymer layer was 50 μm. The measured thermal conductivity and diffusivity of the polyurethane layer were 0.48 W/K $\cdot$ m and 2.7×10^{-7} m^2/s, respectively. The model was made of stainless steel. In image processing, the raw flow-off and flow-on TSP images are corrected by subtracting the background intensity that is contributed by the ambient light and leakage of the optical filter before taking a ratio between the flow-off and flow-on images. Then the ratio images are converted to the temperature images by using a priori calibration data. Figure 9 shows a typical surface temperature image selected from a total of 16 images in the run and the averaged heat flux image in an interval of 4–6 ms in which the flow was stabilized. The surface temperature is obtained by using the iterative relation equation (10) from the TSP-measured temperature. Figure 10 shows three iterations for correction of the surface temperature by Eq. (10) at the maximum heat flux location. The temperature correction for this case is significant due to a high heat transfer rate, and three iterations seem sufficient in this case. Figure 11 shows the heat flux distributions obtained by using the analytical method, Eq. (3), from 16 points and 100 points interpolated from 16 points in comparison with the data given by an array of thin-film heat flux gauges. The heat flux in Fig. 11 is the

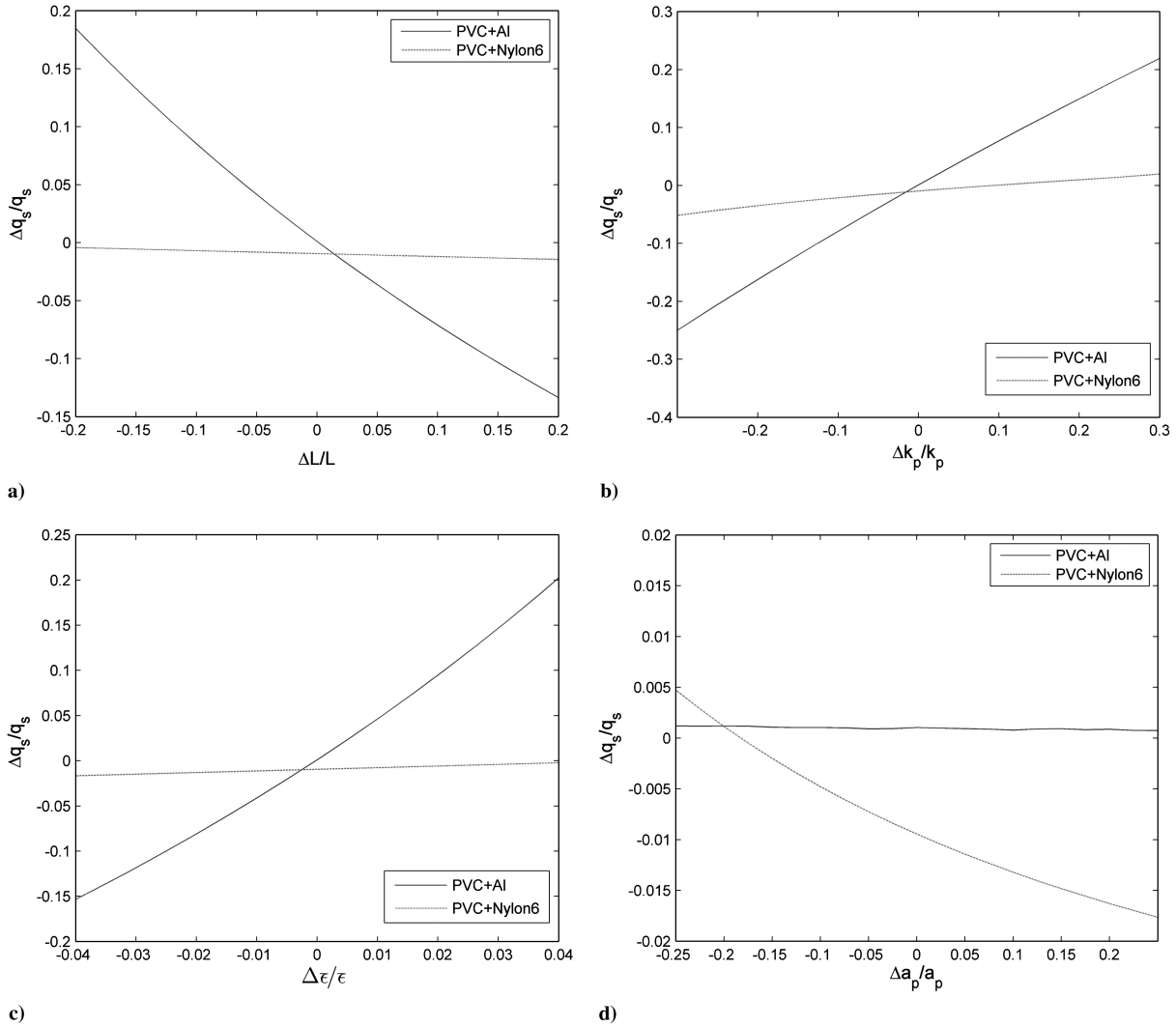

Fig. 7 Uncertainty of heat flux calculated by using the general method for a 0.05 mm PVC layer on a semi-infinite aluminum and nylon 6 bases responding to a step change of heat flux, that results from the elemental errors of a) polymer thickness, b) thermal conductivity, c) $\bar{\epsilon}$, and d) thermal diffusivity.

averaged value in an interval of 4–6 ms in which the flow was stabilized. The interpolation from 16 points gives an improved result, as indicated in the simulations. Note that the results from TSP are not in-situ-corrected.

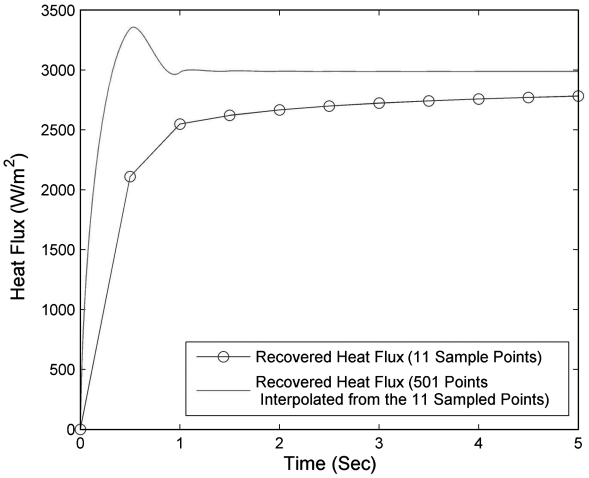

Fig. 8 Improved results based on 501 points obtained from interpolation of 21 sample points in temperature for a 0.1-mm-thick PVC layer on a semi-infinite nylon 6.

B. Boeing/AFOSR Mach-6 Quiet Tunnel

TSP measurements on a nylon cone were conducted in the Boeing/AFOSR Mach-6 Quiet Tunnel at Purdue University [20]. The TSP, Ru(bpy) in Chromaclear auto paint, was directly coated on the nylon surface. The stagnation temperature and pressure were 160°C and 255 psia, respectively. Figure 12a is a raw TSP image of the nylon cone with a surface roughness element triggering boundary-layer transition at Mach 6. Figure 12b shows the averaged heat flux image from $t = 0.5$ to 4 s, which is downsampled over windows of 3×3 pixels to reduce the data processing time. A turbulent wedge triggered by the roughness element is visible, due to the difference between the turbulent and laminar flow regimes. Figure 13 shows typical time histories of the surface temperature and heat flux at $(x, y) = (25, 35)$ pixels in the turbulent wedge and $(x, y) = (15, 25)$ pixels in the laminar boundary layer (reference Fig. 12b for the two positions). The transient starting process of the tunnel is observed in Fig. 13. By assuming that the TSP has the same thermal properties as Mylar and that the TSP thickness is 40 μm, the heat flux is calculated by using Eq. (3) from 45 points and 300 points interpolated from 45 points. In this case, the interpolation does not show a significant improvement, and it indicates that 45 points are sufficient for heat flux calculation using Eq. (3).

C. Infrared Laser Heating

Infrared laser heating on a base provides a simple bench test in a laboratory to simulate the time-dependent heat flux in hypersonic tunnels.

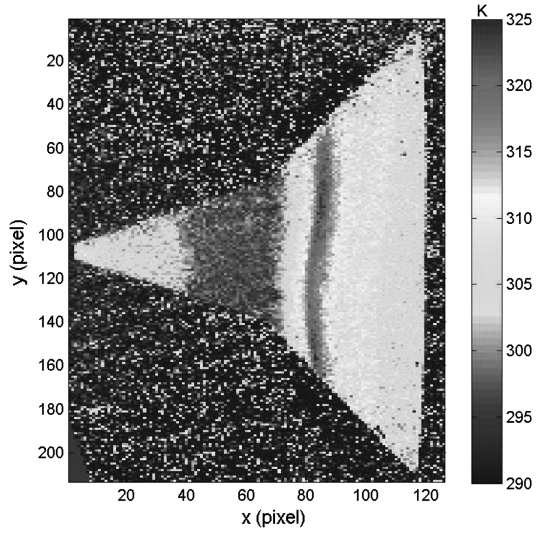

a)

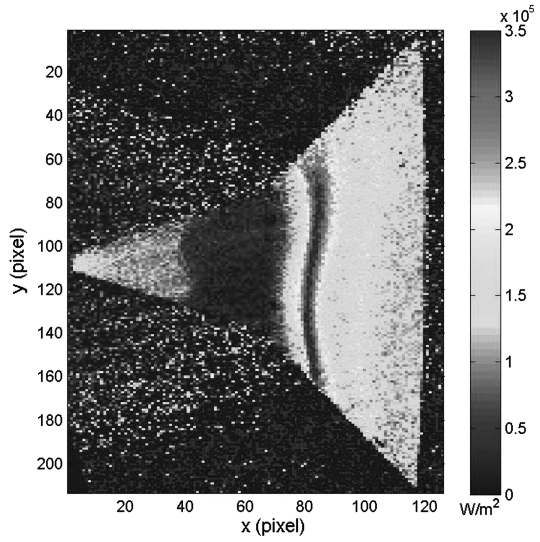

b)

Fig. 9 Images of a) temperature and b) averaged heat flux of the sharp 25 deg /45 deg indented cone model at Mach 11 (the original TSP images from Hubner et al. [2]).

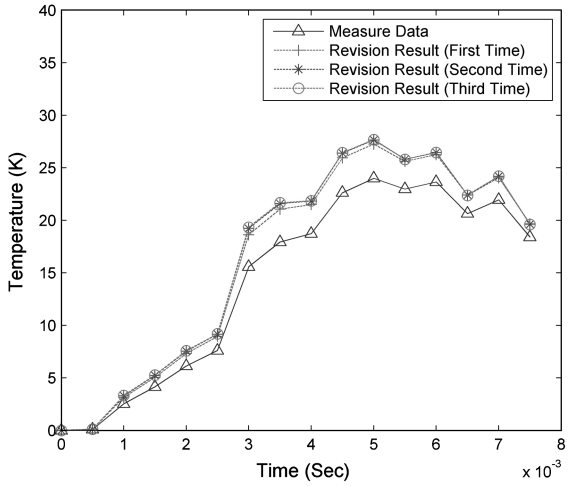

Fig. 10 Three iterations for correction of the surface temperature at the maximum heat flux location.

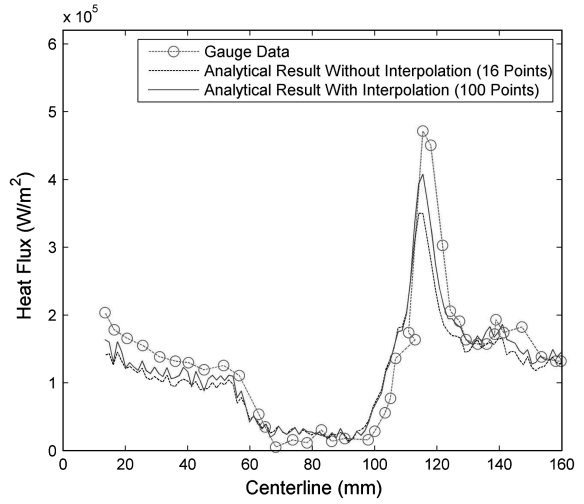

Fig. 11 Heat flux distributions from TSP data along a ray on the sharp 25 deg /45 deg indented cone model at Mach 11 in comparison with the data from an array of thin-film heat flux gauges (the gauge data from Hubner et al. [2]).

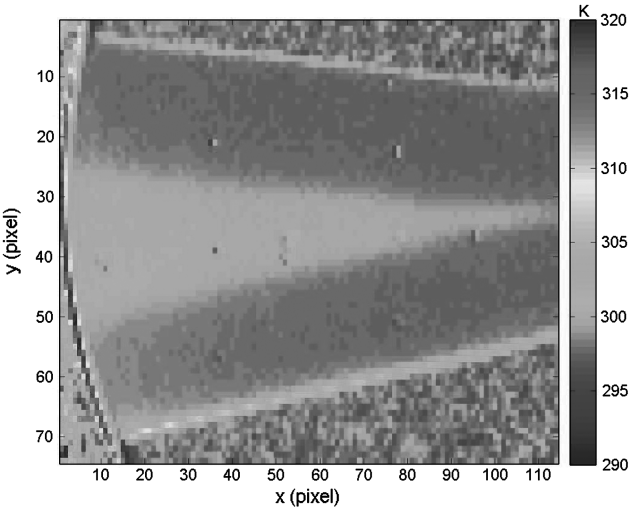

a)

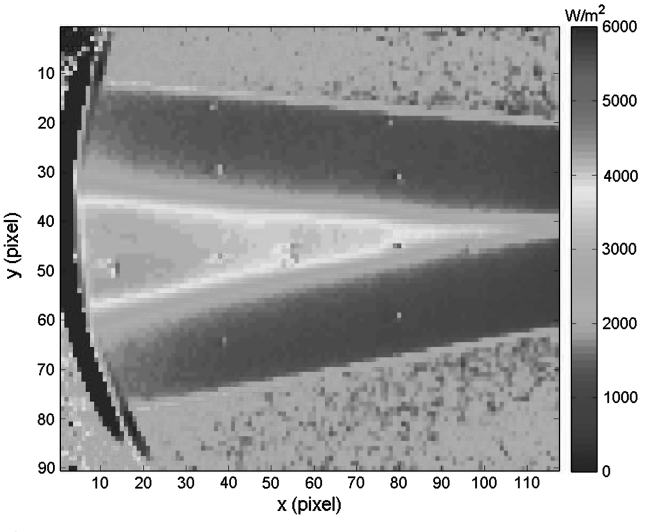

b)

Fig. 12 Images of a) temperature and b) averaged heat flux of a nylon cone with a roughness element at Mach 6.

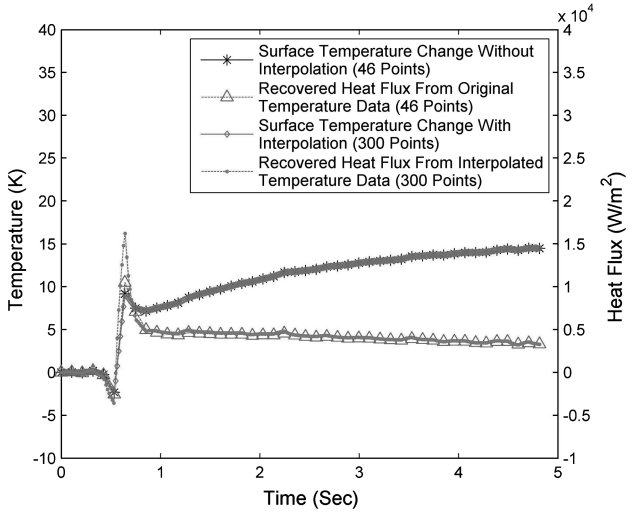

a)

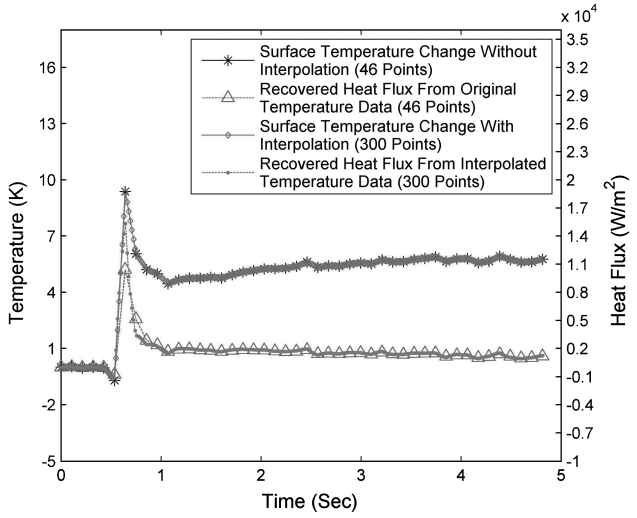

b)

Fig. 13 Typical time histories of the surface temperature and heat flux at a point in the a) turbulent wedge triggered by a roughness element and b) laminar boundary layer.

As illustrated in Fig. 14, the sample was made of substrate, an insulator, and a layer of TSP. Substrates used were nylon, aluminum, and PVC. Vinyl electrical tape and black Mylar were used as an insulating layer. The dark color decreases the signal returned to the camera, but increases absorption of the IR laser. Before each run the laser was turned on and allowed to warm up while a shutter prevented

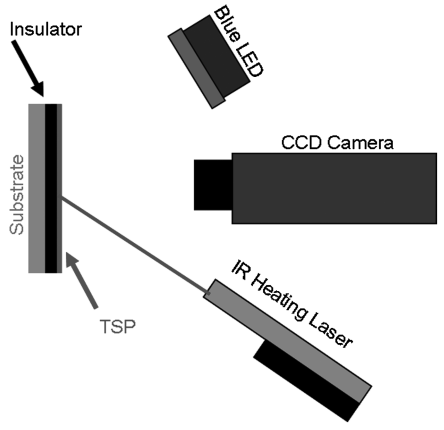

Fig. 14 Infrared laser heating setup.

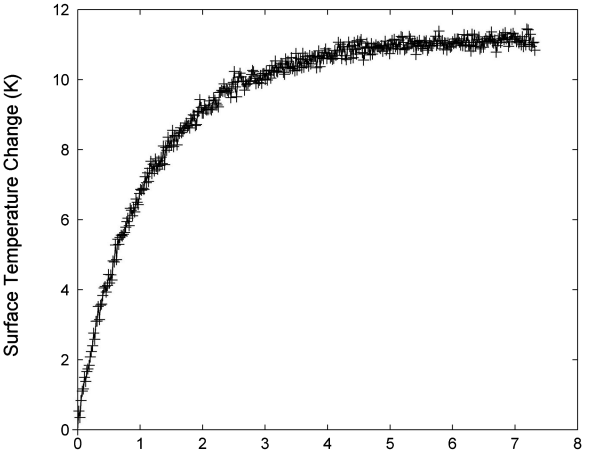

a)

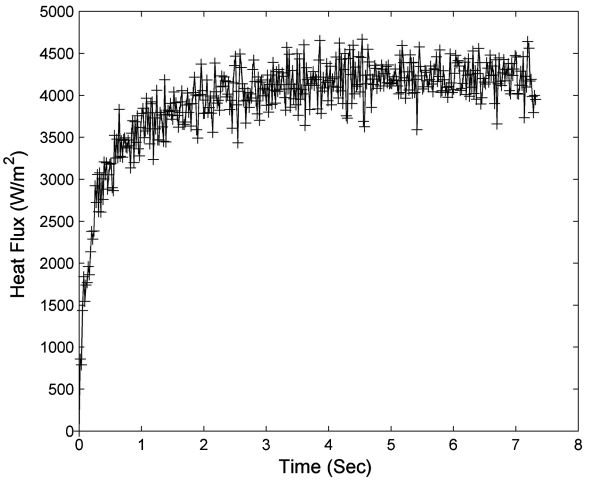

b)

Fig. 15 Step laser heating: a) the surface temperature and b) the recovered surface heat flux as a function time at the center of the heated spot.

the laser from reaching the sample. Then the shutter was removed as the camera was recording images. The first test was step heating provided by an IR laser with a 0.3 o.d. filter of 0.2 cm thickness to reduce the power of the laser. The substrate was 0.5-in.-thick aluminum and the insulator was 600-μm-thick electrical tape. The thermal conductivity and diffusivity of the insulating layer are 0.15 $\mathrm{W/m \cdot K}$ and 9.7×10^{-8} $\mathrm{m^2/s}$, respectively. The ambient temperature was 77°F. Figure 15 shows a typical time history of the surface temperature and the recovered heat flux at the center of the heated spot. The large temporal variation in the calculated heat flux in Fig. 15b indicates that the result is sensitive to a noise in the time derivative calculation in Eq. (1) or Eq. (3). This phenomenon is

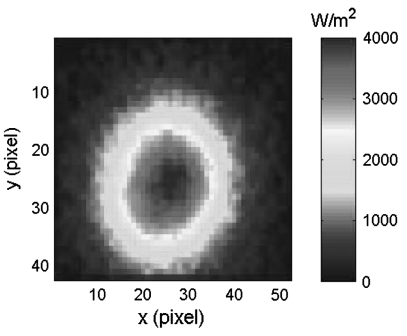

Fig. 16 Time-averaged heat flux distribution in the step laser heating.

typical in inverse problems. Figure 16 shows the time-averaged heat flux distribution in the step laser heating. The recovered heat flux is not exactly a step function, because the thick insulating layer has a large time constant. Periodically oscillating laser heating was also measured. The surface temperature increases gradually during the heating while it oscillates. The peaks and valleys of the recovered surface heat flux remain the same level, which is reasonable.

VII. Conclusions

The exact inverse solution of the 1-D time-dependent heat conduction equation is obtained by using the Laplace transform for a thin polymer (TSP or TSP/insulator layer) on a semi-infinite base. This solution leads to the analytical method for determining heat flux from a time history of the surface temperature measured by TSP in hypersonic tunnels. Simulations indicate that the analytical method is able to determine a complicated transient heat flux history as along as the intrinsic response time of TSP is sufficiently small. The heat flux recovered by the analytical method is independent of a complicated tunnel-starting process after a transient process. Therefore, the analytical method can be used for various hypersonic tunnels with different starting characteristics. The uncertainty of heat flux calculation is contributed by the elemental errors such as the polymer thickness, thermal conductivity, thermal diffusivity, and ratio of the thermal properties between the polymer and base. The sensitivity of calculated heat flux to the elemental sources for a low-thermal-conductive base is much weaker than that for a metal base. Data interpolation from a small sample group can improve the accuracy of heat flux calculation. An iterative scheme for the polymer surface temperature from the TSP-measured temperature could improve the accuracy of heat flux measurement, particularly when heat flux is very large. To examine the analytical method, TSP images on a sharp 25 deg /45 deg indented metal cone model at Mach 11 are reprocessed, and the recovered heat flux results are in good agreement with those measured by thin-film heat flux gauges. Furthermore, the analytical method is applied to TSP measurements on a nylon cone at Mach 6, and the recovered heat flux field indicates a turbulent wedge triggered by a roughness element on the cone surface. The results in IR laser heating as a bench test are also presented.

Appendix A: Analytical Solutions

I. Heat Conduction Equation and Laplace Transform

A transient solution of the 1-D time-dependent heat conduction equation is sought by using the Laplace transform. Because a polymer layer is usually thin, the 1-D time-dependent heat conduction equation can be used, assuming that the lateral heat conduction can be neglected. The heat conduction equation for a polymer layer is

$$\left(\frac{\partial}{\partial t} - a_p \frac{\partial^2}{\partial y^2}\right)\theta_p(t, y) = 0 \tag{A1}$$

where $\theta_p(t, y) = T_p - T_{\text{in}}$ is a temperature change in the polymer layer from a constant initial temperature T_{in}, and $a_p = k_p/c_p\rho_p$ is the thermal diffusivity of the polymer. Here, k_p, c_p, and ρ_p are the thermal conductivity, specific heat, and density of the polymer. Similarly, the governing equation for the base is

$$\left(\frac{\partial}{\partial t} - a_b \frac{\partial^2}{\partial y^2}\right)\theta_b(t, y) = 0 \tag{A2}$$

where $\theta_b(t, y) = T_b - T_{\text{in}}$ is a temperature change of the base from a constant initial temperature, and $a_b = k_b/c_b\rho_b$ is the thermal diffusivity of the base (k_b, c_b and ρ_b are the thermal conductivity, specific heat, and density of the base, respectively). It is assumed that both the polymer layer and base have the same initial temperature. Here, the thermal properties are considered to be constant for both the polymer layer and base. When the thermal diffusivity k is temperature-dependent, the Kirchhoff's model temperature can be introduced such that the form of Eq. (A1) or (A2) remains unchanged [21].

The boundary condition at the polymer surface is

$$q_s(t) - k_p \frac{\partial}{\partial y}\theta_p(t, L) = 0 \tag{A3}$$

where $q_s(t)$ is the heat flux into the polymer surface and L is the polymer-layer thickness. The boundary condition at infinity in the base is

$$\theta_b(t, -\infty) = 0 \tag{A4}$$

The matching conditions at the interface between the polymer and base are

$$\theta_p(t, 0) = \theta_b(t, 0) \tag{A5}$$

and

$$k_p \frac{\partial}{\partial y}\theta_p(t, 0) = k_b \frac{\partial}{\partial y}\theta_b(t, 0) \tag{A6}$$

After applying the Laplace transform

$$\Theta_p(s, y) = \int_0^\infty \theta_p(t, y) \exp(-st)\, \mathrm{d}t \tag{A7}$$

Eq. (A1) becomes

$$\frac{\mathrm{d}^2\Theta_p}{\mathrm{d}y^2} = \frac{s}{a_p}\Theta_p(s, y) \tag{A8}$$

Similarly, the transformed form of Eq. (A2) is

$$\frac{\mathrm{d}^2\Theta_b}{\mathrm{d}y^2} = \frac{s}{a_b}\Theta_b(s, y) \tag{A9}$$

The solutions for Eqs. (A8) and (A9) are obtained and the corresponding transformed boundary and matching conditions are applied to determine the unknown coefficients. Therefore, the transformed heat flux at the polymer surface is given by

$$Q_s(s) = k_p\sqrt{s/a_p}\,\Theta_{ps}(s)G(s) \tag{A10}$$

where $\Theta_{ps}(s) = \Theta_p(s, L)$ is the transformed temperature change at the polymer surface. The function $G(s)$ is defined by

$$G(s) = \frac{1 + \bar{\varepsilon}\exp(-2L\sqrt{s/a_p})}{1 - \bar{\varepsilon}\exp(-2L\sqrt{s/a_p})} \tag{A11}$$

where $\bar{\varepsilon} = (1 - \varepsilon)/(1 + \varepsilon)$ and $\varepsilon = \sqrt{k_p\rho_p c_p/k_b\rho_b c_b}$. Now the main problem is how to obtain an inverse Laplace transform of Eq. (A10) for the heat flux into the polymer surface as a function of the polymer surface temperature change. The effect of the base is contained in Eq. (A11).

II. Inversion of Laplace Transform for General Case

The inversion of Eq. (A10) for a general case is sought. Equation (A10) is written as

$$Q_s(s) = (k_p/\sqrt{a_p})s\Theta_{ps}(s)K(s) \tag{A12}$$

where

$$K(s) = \frac{1}{\sqrt{s}}\frac{1 + \bar{\varepsilon}\exp(-2L\sqrt{s/a_p})}{1 - \bar{\varepsilon}\exp(-2L\sqrt{s/a_p})} \tag{A13}$$

The inversion of $K(s)$ is

$$k(t) = \frac{1}{2\pi i}\int_{\gamma - i\infty}^{\gamma + i\infty} \exp(st)K(s)\, \mathrm{d}s \tag{A14}$$

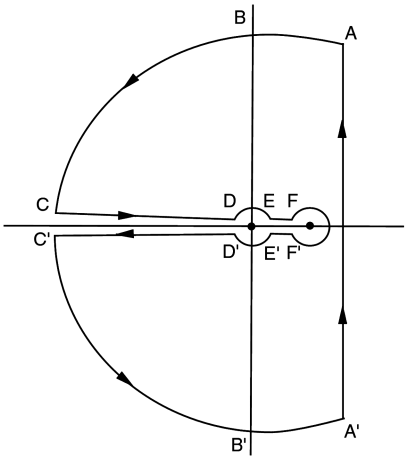

Fig. A1 Contour for inversion of the Laplace transform.

To calculate the inversion, following a standard procedure [22,23], we consider a contour integral

$$I = \int \exp(st)K(s)\,\mathrm{d}s \tag{A15}$$

The function $K(s)$ has a branch point at $s = 0$ and a pole at $s = i^4(a_p/4L^2)|\ln \bar{\varepsilon}|^2$.

The integral Eq. (A15) along a closed contour C illustrated in Fig. A1 is zero. The integral $I_{A'A}$ over the segment $A'A$ approaches the integral in Eq. (A15) as the radius R of a large circle goes to infinity, where A and A' are at $\gamma + i\beta$ and $\gamma - i\beta$, respectively. For the segment AB, $s = R\exp(i\theta)$, where $\tan^{-1}(\beta/\gamma) \le \theta \le \pi/2$, and $|K(s)| < CR^{-1/2}$ as $R \to \infty$. Therefore, $I_{AB} \to 0$ as $R \to \infty$. Similarly, $I_{A'B'} \to 0$, $I_{BC} \to 0$, and $I_{C'B'} \to 0$ as $R \to \infty$. For the segments CD and $D'C'$, $s = r\exp[i(\pi - \delta)]$ and $s = r\exp[i(-\pi + \delta)]$ as $\delta \to 0$, respectively. After some arrangements, we have the integral

$$I_{CD} + I_{D'C'} = \frac{2(1-\bar{\varepsilon}^2)}{i}\int_{r_0}^{R}\frac{\exp(-rt)}{\sqrt{r}}\frac{\mathrm{d}r}{1+\bar{\varepsilon}^2 - 2\bar{\varepsilon}\cos(2L\sqrt{r/a_p})} \tag{A16}$$

where r_0 is the radius of a small circle around a branch point at $s = 0$. The limits $r_0 \to 0$ and $R \to \infty$ will be taken in Eq. (A16). For the segments EF [$s = r\exp(i\delta)$ as $\delta \to 0$] and $F'E'$ [$s = r\exp(-i\delta)$ as $\delta \to 0$], $I_{EF} + I_{F'E'} = 0$. For a circular contour $DEE'D'$ [$s = r_0\exp(i\theta)$, where $\theta = \pi$ to $-\pi$], $I_{DEE'D'} \to 0$ as $r_0 \to 0$. Similarly, for a circular contour FF' [$s = r_0\exp(i\theta)$, where $\theta = \pi$ to $-\pi$], $I_{FF'} \to 0$ as $r_0 \to 0$. Combining the integrals along all the segments of the contour C, we obtain

$$k(t) = (\sqrt{a_p}/L)W(t) \tag{A17}$$

where

$$W(t) = \frac{1-\bar{\varepsilon}^2}{\pi}\int_0^{\infty}\frac{\exp[-(a_p t/4L^2)\eta^2]\,\mathrm{d}\eta}{1+\bar{\varepsilon}^2 - 2\bar{\varepsilon}\cos\eta} \tag{A18}$$

Therefore, the heat flux at the polymer surface is

$$q_s(t) = \frac{k_p(1-\bar{\varepsilon}^2)}{\sqrt{\pi a_p}}\int_0^t \frac{\bar{W}(t-\tau,\bar{\varepsilon})}{\sqrt{t-\tau}}\,\frac{\mathrm{d}\theta_{ps}(\tau)}{\mathrm{d}\tau}\,\mathrm{d}\tau \tag{A19}$$

where

$$\bar{W}(t,\bar{\varepsilon}) = \frac{2}{\sqrt{\pi}}\int_0^{\infty}\frac{\exp(-\xi^2)\,\mathrm{d}\xi}{1+\bar{\varepsilon}^2 - 2\bar{\varepsilon}\cos(2L\xi/\sqrt{a_p t})} \tag{A20}$$

III. Effect of Lateral Heat Conduction

We consider the 3-D heat conduction equation for a polymer layer

$$\frac{\partial\theta_p}{\partial t} = a_p\left(\frac{\partial^2\theta_p}{\partial x^2} + \frac{\partial^2\theta_p}{\partial y^2} + \frac{\partial^2\theta_p}{\partial z^2}\right) \tag{A21}$$

where y is the coordinate normal to the surface between the polymer layer and base, and x and z are the coordinates on the surface. Using the Fourier transform to Eq. (A21),

$$\hat{\theta}_p = \int_{-\infty}^{\infty}\int_{-\infty}^{\infty}\theta_p\exp(-i[ux+vz])\,\mathrm{d}x\,\mathrm{d}z \tag{A22}$$

Eq. (A21) becomes

$$\frac{\partial\hat{\theta}_p}{\partial t} = a_p\left(\frac{\partial^2\hat{\theta}_p}{\partial y^2} - (u^2+v^2)\hat{\theta}_p\right) \tag{A23}$$

where $\hat{\theta}_p = \hat{\theta}_p(t,y,u,v)$. Further, applying the Laplace transform to Eq. (A23),

$$\hat{\Theta}_p(s,y) = \int_0^{\infty}\hat{\theta}_p(t,y)\exp(-st)\,\mathrm{d}t \tag{A24}$$

Eq. (A23) becomes

$$\frac{\mathrm{d}^2\hat{\Theta}_p}{\mathrm{d}y^2} = [s/a_p + (u^2+v^2)]\hat{\Theta}_p \tag{A25}$$

In a similar way to the 1-D analysis, considering the matching conditions at the interface, we have the transformed heat flux at the polymer surface:

$$\hat{Q}_s(s,u,v) = \frac{k_p}{\sqrt{a_p}}[s + a_p(u^2+v^2)]\hat{\Theta}_{ps}(s,u,v)K(s',u,v) \tag{A26}$$

where $\hat{\Theta}_p(s,L,u,v)$ is the transformed temperature change at the polymer surface. The function $K(s',u,v)$ is defined by

$$K(s',u,v) = \frac{1}{\sqrt{s'}}\frac{1+\bar{\varepsilon}\exp(-2L\sqrt{s'/a_p})}{1-\bar{\varepsilon}\exp(-2L\sqrt{s'/a_p})} \tag{A27}$$

where $s' = s + a_p(u^2+v^2)$, $\bar{\varepsilon} = (1-\varepsilon)/(1+\varepsilon)$, and $\varepsilon = \sqrt{k_p\rho_p c_p/k_b\rho_b c_b}$. The inverse Laplace transform of $K(s',u,v)$ is

$$\begin{aligned} k(t,u,v) &= \frac{1}{2\pi i}\int_{\gamma-i\infty}^{\gamma+i\infty}\exp(st)K(s',u,v)\,\mathrm{d}s \\ &= \frac{\exp[-a_p(u^2+v^2)t]}{2\pi i}\int_{\gamma'-i\infty}^{\gamma'+i\infty}\exp(s't)K(s',u,v)\,\mathrm{d}s' \end{aligned} \tag{A28}$$

Because the integral in Eq. (A28) is the same as Eq. (A14), the result of the contour integral of (A18) can be directly used; that is,

$$k(t,u,v) = (\sqrt{a_p}/L)\exp[-a_p(u^2+v^2)]W(t)$$

Therefore, the inverse Laplace transform of Eq. (A28) leads to

$$\begin{aligned} \hat{q}_s(t,u,v) = \frac{k_p}{L}\Bigg[&\int_0^t W(t-\tau)\exp[-a_p(u^2+v^2)(t-\tau)]\frac{\mathrm{d}\hat{\theta}_{ps}}{\mathrm{d}\tau}\,\mathrm{d}\tau \\ &+ a_p(u^2+v^2)\int_0^t W(t-\tau)\exp[-a_p(u^2+v^2)(t-\tau)]\hat{\theta}_{ps}\,\mathrm{d}\tau\Bigg] \end{aligned} \tag{A29}$$

Further, the inverse Fourier transform of Eq. (A29) yields Eq. (4) for the heat flux at the polymer surface.

Acknowledgments

This work is supported by a NASA Research Announcement grant (NNX08AC97A). We would like to thank Steven Schneider and his group for collaborations in measurements in The Boeing Company and U.S. Air Force Office of Scientific Research Mach-6 Quiet Tunnel at Purdue University. We are grateful to Paul Hubner for kindly providing the original temperature-sensitive-paint images obtained in the 48 in. shock tunnel and relevant information on their experiments conducted at Calspan–University of Buffalo Research Center.

References

[1] Liu, T., Campbell, B., and Sullivan, J., "Heat Transfer Measurement on a Waverider at Mach 10 Using Fluorescent Paint," *Journal of Thermophysics and Heat Transfer*, Vol. 9, No. 4, 1995, pp. 605–611. doi:10.2514/3.714

[2] Hubner, J. P., Carroll, B. F., and Schanze, K. S., "Heat-Transfer Measurements in Hypersonic Flow Using Luminescent Coating Techniques," *Journal of Thermophysics and Heat Transfer*, Vol. 16, No. 4, 2002, pp. 516–522. doi:10.2514/2.6726

[3] Norris, J. D., Hamner, M., Lafferty, J. F., Smith, N. T., and Lewis, M. J., "Adapting Temperature-Sensitive Paint Technology for Use in AEDC Hypervelocity Wind Tunnel 9," AIAA Paper 2004-2191, Portland, OR, 2004.

[4] Kurits, I., Lewis, M., Hamner, M., and Norris, J. D., "Development of a Global Heat Transfer Measurement System at AEDC Hypervelocity Wind Tunnel 9," *International Congress on Instrumentation in Aerospace Simulation Facilities*, Inst. of Electrical and Electronics Engineers, Piscataway, NJ, 2007.

[5] Matsumura, S., Berry, S. A., and Schneider, S. P., "Flow Visualization Measurement Techniques for High-Speed Transition Research in the Boeing/AFOSR Mach-6 Quiet Tunnel," AIAA Paper 2003-4583, July 2003.

[6] Matsumura, S., Schneider, S. P., and Berry, S. A., "Streamwise Vortex Instability and Transition on the Hyper-2000 Scramjet Forebody," *Journal of Spacecraft and Rockets*, Vol. 42, No. 1, 2005, pp. 78–88. doi:10.2514/1.3959

[7] Schneider, S. P., Rufer, S., Skoch, C., and Swanson, E., "Hypersonic Transition Research in the Boeing/AFOSR Mach-6 Quiet Tunnel," AIAA Paper 2003-3450, June 2003.

[8] Liu, T., and Sullivan, J., *Pressure and Temperature Sensitive Paints*, Springer, Berlin, 2004.

[9] Schultz, D. L., Jones, T. V., "Heat transfer measurements in short-duration hypersonic facilities," AGARDograph No. 165, 1973.

[10] Merski, N. R., "Reduction and Analysis of Phosphor Thermography Data with the IHEAT Software Package," AIAA Paper 98-0712, 1998.

[11] Merski, N. R., "Global Aeroheating Wind-Tunnel Measurements Using Improved Two-Color Phospher Thermography Method," *Journal of Spacecraft and Rockets* Vol. 36, No. 2, 1999, pp. 160–170. doi:10.2514/2.3446

[12] Alifanov, O. M., *Inverse Heat Transfer Problems*, Springer–Verlag, Berlin, 1994, Chaps. 1, 2.

[13] Beck, J. V., Blackwell, B., and St. Clair, C. R., Jr., *Inverse Heat Conduction: Ill-Posed Problem*, Wiley-Interscience, New York, 1985.

[14] Walker, D. G., and Scott, E. P., "Evaluation of Estimation Methods for High Unsteady Heat Fluxes from Surface Measurements," *Journal of Thermophysics and Heat Transfer*, Vol. 12, No. 4, 1998, pp. 543–551. doi:10.2514/2.6374

[15] Smith, R. H., Scott, E. P., and Ligrani, P. H., "Experimental Validation of an Inverse Heat Conduction Problem Using Thermocouple and Infrared Data," AIAA Paper 2001-0507, Reno, NV, 2001.

[16] Kojima, F., Fukuda, S., Asai, K., and Nakakita, K., "Identification of Time and Spatial Varying Heat Flux from Surface Measurements Based on Temperature-Sensitive Paint Technology," *SICE Annual Conference in Sapporo*, Society of Instrument and Control Engineers, Aug. 2004.

[17] Estorf, M., "Image Based Heating Rate Calculation from Thermographic Data Considering Lateral Heat Conduction," *International Journal of Heat and Mass Transfer*, Vol. 49, Nos. 15–16, July 2006, pp. 2545–2556. doi:10.1016/j.ijheatmasstransfer.2005.12.018

[18] Cook, W. J., and Felderman, E. J., "Reduction of Data from Thin-Film Heat Transfer Gages: A Concise Technique," *AIAA Journal*, Vol. 8, No. 7, 1970, pp. 1366–1368. doi:10.2514/3.5909

[19] Liu, T., Cai, Z., Lai, J., Rubal, J., and Sullivan, J., "Analytical Methods for Determination of Heat Transfer Fields from Temperature Sensitive Paint Measurements in Hypersonic Tunnels," AIAA Paper 2009-0736, Orlando, FL, 2009.

[20] Casper, K. M., Wheaton, B. M., Johnson, H. B., and Schneider, S. P., "Effects of Freestream Noise on Roughness-Induced Transition at Mach 8," AIAA Paper 2008-4291, Seattle, WA, 2008.

[21] Carslaw, H. S., and Jaeger, J. C., "*Conduction of Heat in Solids*," 2nd ed., Oxford Univ. Press, Oxford, 2000, Chap. 1.

[22] Carslaw, H. S., and Jaeger, J. C., *Operational Methods in Applied Mathematics*, Dover, New York, 1963, Chap. 4.

[23] Smith, M. G., *Laplace Transform Theory*, D. Van Nostrand, London, 1966, Chap. 4.